Lab on a Chip

PAPER

View Article Online
View Journal

Cite this: DOI: 10.1039/d5lc01167a

High-throughput microfluidic platform for modelling inflammatory responses of human articular chondrocytes under variable fluid shear stress

Aldeliane M. da Silva, [a] Priscila Campioni Rodrigues, [a] Meriem Lamghari,[b] Hoang-Tuan Nguyen, [c] Jere Kettunen,[c] Sebastien Mosser,[c] Prateek Singh,[c] Ali Mobasheri [defghi] and Gabriela S. Lorite *[a]

Inflammation plays a critical role in osteoarthritis (OA), a debilitating joint disease characterized by cartilage degradation, chronic pain, and disability. The absence of approved disease-modifying OA drugs underscores the need for physiologically relevant *in vitro* models to accelerate preclinical screening. Cartilage-on-chip platforms integrating 3D matrices and mechanical cues have emerged as promising tools to replicate cartilage microenvironments and OA phenotypes; however, their complexity limits scalability for high-throughput applications. Here, we exploited and optimized a streamlined, pumpless microfluidic system enabling dynamic culture of human articular chondrocytes under controlled gradients of fluid shear stress and cytokine-induced inflammation. Each chip accommodates 24 replicates and generates shear stresses ranging from 0.06 to 0.9 Pa. The platform supports long-term culture of healthy chondrocytes, maintaining high viability, enhanced collagen type II and aggrecan expression, and formation of 3D aggregates and contracted microtissue-like structures over 21 days. Inflammatory conditions induced by stimulation with recombinant interleukin-1β (IL-1β) led to extracellular matrix degradation, disrupted tissue architecture, and reduced expression of cartilage-specific markers. Elevated levels of metalloproteinases and pro-inflammatory cytokines, characteristics of OA, were detected even at minimal IL-1β concentrations, demonstrating the model's sensitivity to inflammatory stimuli. This microfluidic system provides a robust, scalable approach for modeling OA-related inflammation in a dynamic environment, offering strong potential for high-throughput drug screening targeting inflammatory pathways.

Received 19th December 2025,
Accepted 7th April 2026

DOI: 10.1039/d5lc01167a

rsc.li/loc

1. Introduction

Articular cartilage (AC) is a specialized connective tissue composed of chondrocytes embedded in a dense extracellular matrix (ECM) rich in water, collagen fibrils, proteoglycans, and glycosaminoglycans.[1,2] AC experiences diverse mechanical forces, including compression, tensile stress, interstitial fluid pressure, and fluid-induced shear stress (FSS) generated by synovial fluid flow. Its zonal architecture, including superficial, middle, and deep layers, confers distinct mechanical properties: the superficial zone primarily resists shear forces, while deeper zones withstand compressive loads.[3,4] This structural complexity enables AC to distribute mechanical loads, minimize friction, and protect subchondral bone during joint movement.

Chondrocytes, the sole cellular component of AC, are highly mechanosensitive and regulate ECM synthesis and cartilage homeostasis in response to mechanical cues.[1–5] Disruption of this balance by excessive mechanical stress or

[a] Microelectronics Research Unit, University of Oulu, Pentti Kaiteran Katu 1, 90014, Oulu, Finland. E-mail: gabriela.lorite@oulu.fi
[b] i3S – Instituto de Inovação e Investigação em Saúde, INEB – Instituto Nacional de Engenharia Biomédica, Universidade do Porto, Rua Alfredo Allen, 208, Porto 4200-135, Portugal
[c] Finnadvance, Viikinkaari 1, Biokeskus 3, 00790 Helsinki, Finland
[d] Research Unit of Health Sciences and Technology, Faculty of Medicine, University of Oulu, Oulu, Finland
[e] Department of Personalized Medicine, State Research Institute Centre for Innovative Medicine, Vilnius, Lithuania
[f] Department of Joint Surgery, The First Affiliated Hospital of Sun Yat-sen University, Guangdong, China
[g] Faculté de Médecine, Université de Liège, Liège, Belgium
[h] Department for Health Sciences, Medicine and Research, Center for Regenerative Medicine, Faculty of Health and Medicine, University for Continuing Education Krems, Krems, Austria
[i] Department of Orthopedic Surgery, Maastricht University Medical Center, Maastricht, The Netherlands

inflammation leads to chondrocyte dysfunction and ECM degradation, hallmark features of osteoarthritis (OA), a progressive joint disease affecting over 500 million people worldwide.[1–5] With aging as a major risk factor, OA prevalence and socioeconomic burden are expected to rise sharply. Despite its growing impact, no disease-modifying OA drugs (DMOADs) are currently available, and treatment options remain limited to symptom management or surgical intervention. A major obstacle to therapeutic development is the lack of physiologically relevant preclinical models.[5–7]

Conventional drug screening platforms rely heavily on two-dimensional (2D) *in vitro* systems and animal models.[8] While these approaches have provided valuable insights into disease mechanisms, they fail to replicate the human-specific biochemical and biomechanical environment of cartilage.[6–8] Traditional 2D cultures oversimplify the cartilage microenvironment, whereas animal models, although more integrative, often do not accurately reproduce human disease processes or drug responses due to interspecies differences.[8–10] These limitations have driven the development of advanced *in vitro* systems, including synthetic hydrogels,[11–15] 3D scaffolds,[16,17] organoids,[18,19] and organ-on-chip (OoC) devices, which have emerged as transformative technologies integrating microfluidics, 3D cell culture, and mechanical stimulation to better mimic native tissue physiology and disease states.[20–27]

OoC devices for articular cartilage have incorporated pneumatic compression,[28–34] and magnetically-responsive hydrogels[35] to apply dynamic mechanical load in chondrocytes embedded in hydrogel matrices at both physiological and hyper-physiological levels to induce OA-like phenotypes. These technologies represent a paradigm shift toward physiologically relevant models for studying cartilage pathophysiology and improving the predictive accuracy of preclinical drug screening. While these approaches successfully replicate biomechanical environments, they are inherently complex due to the reliance on peripheral equipment for fluidic connections and air pressurization in the case of pneumatic actuated systems, limiting scalability and high-throughput applications. Alternatively, *in vitro* platforms for modelling OA have been developed by inducing inflammation with pro-inflammatory cytokines, such as recombinant IL-1β.[36–39] This strategy has been employed in 2D models, spheroids and few OoC systems to study inflammation in joint tissues, including cartilage, bone, and synovium.[36–40] Despite the potential of these OoC models in mimicking OA, challenges related to scalability, application in high-throughput studies and drug development still remain.

FSS naturally present in AC due to synovial fluid flow, is a physiologically relevant mechanical cue that can be precisely controlled in microfluidic systems. Low FSS (<2 Pa) promotes chondrocyte growth and ECM synthesis, whereas high FSS (>15 Pa) impairs cellular function.[41–43] Cartilage is exposed to varying levels of FSS *in vivo*, depending on joint movement and loading conditions. Gradient-based FSS stimulation has been applied to other cell types, such as endothelial cells[44–46] and astrocytes,[47] but no high-throughput platform implementing FSS gradients for human articular chondrocytes has been reported.

In this work, we employed a pumpless microfluidic system, previously designed for endothelial cells derived from induced pluripotent stem cells (iPSC),[44] to enable culture of human articular chondrocytes under controlled FSS gradients.[44] The chip design features microchannels of varying widths to generate distinct shear stress levels (0.06–0.9 Pa) using gravity-driven flow by rocker tilting, eliminating pumps and external tubing for simplified operation and scalability.[47] This platform was optimized for long-term dynamic culture of healthy chondrocytes, enabling assessment of cell viability, metabolic activity, ECM synthesis, and inflammatory responses under FSS as a physiologically relevant mechanical stimulation. Finally, we established an OA-like inflammatory model by stimulating cells with IL-1β, creating a robust and scalable approach for high-throughput screening of candidate DMOADs. This work demonstrates the potential of validated microfluidic systems for cartilage mechanobiology and inflammation research, accelerating the development of physiologically relevant *in vitro* disease models. Additionally, it demonstrated that a microfluidics platform can be effectively adapted and optimized, fostering OoC development across diverse research fields.

2. Materials and methods

2.1 Microfluidic chips and gravity-driven fluid flow

Microfluidic chips containing 24 culture units (Fig. 1A) were fabricated using soft lithography. The design was based on a previously reported platform[44] (Finnadvance Ltd.) that enables spatial variations in FSS across adherent cells within microchannels. Each culture unit comprises two medium inlets connected to reservoirs and four parallel microchannels with progressively decreasing width and height, thereby generating three distinct fluid shear stress (FSS) regions: region I (low FSS), region II (medium FSS), and region III (high FSS) (Fig. 1B). The microchannels have a rectangular cross-section, and the dimensions of each region (length × width × height) are as follows: region I – 1500 × 200 × 200 μm, region II – 1500 × 150 × 150 μm, and region III – 1500 × 100 × 100 μm. 3D-printed resin molds were cast with PDMS at a 1 : 10 crosslinker-to-base ratio. Chips were cured at 65 °C for 4 h, demolded, and sealed with a PDMS film using air plasma bonding. Microchannels were inspected for uniform flow, absence of blockages, and leakage. Chips were then cleaned with 96% ethanol and sterilized under UV light. Bidirectional gravity-driven flow was achieved without external pumps by placing the chip on a rocker platform oscillating between ±25° or ±10° at 1 rpm, with a dwell time of 300 s at each tilt position (Fig. 1C). This configuration allowed straightforward loading of cells and culture medium by pipetting, facilitating scalability. Prior to cell seeding, microchannels were coated by protein adsorption to promote cell adhesion and proliferation (Fig. 1D). Healthy human articular chondrocytes were introduced into the channels and maintained under static conditions for 24 h to enable adhesion. Dynamic culture was then initiated by tilting the rocker plate, and samples were collected at defined time points. Culture conditions were optimized for long-term

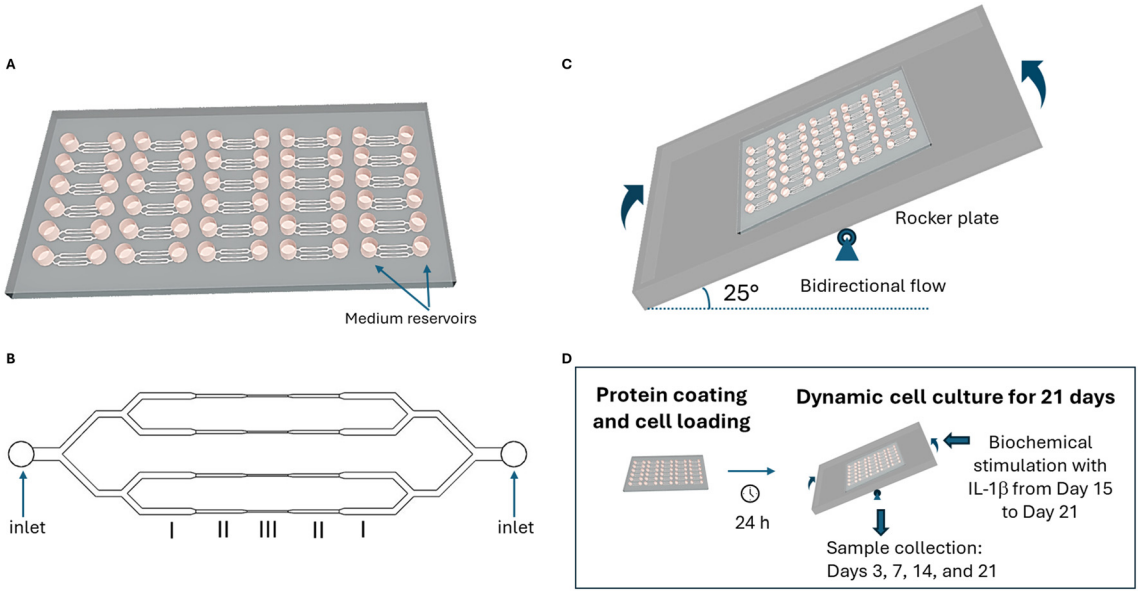

Fig. 1 Schematic representation of the experimental setup: (A) microfluidic chip design comprising 24 culture units, each containing four parallel microchannels of varying widths connected to two medium reservoirs. (B) Detailed view of a single unit showing width variation along the microchannels. Regions I, II, and III correspond to decreasing channel widths, resulting in increasing fluid shear stress, with the highest in region III. (C) Illustration of the rocker plate tilt angle used to generate gravity-driven bidirectional flow during dynamic culture. (D) Overview of the experimental workflow, including cell culture in the microfluidic chip, induction of inflammation with IL-1β, and sample collection at defined time points.

maintenance of healthy chondrocytes. From day 15 to day 21, cells were stimulated with IL-1β (1 ng mL^{-1} or 10 ng mL^{-1}) to induce a pro-inflammatory phenotype resembling osteoarthritic chondrocytes (Fig. 1D).

Gravity-driven flow in the microfluidic channel was generated under asymmetric initial loading conditions, where one medium reservoir was fully filled and the other reservoir was half-filled. Considering $t = 0$ when the rocker was tilted to the angle α, a hydrostatic imbalance developed between the reservoirs generating a pressure drop across the channel $\Delta P_0 = \rho g \Delta h_0$, with ρ denoting fluid density and gravitational acceleration. During the dwell time, with the rocker plate at fixed angle α, the flow rate depends on the pressure drop and is influenced by the hydraulic resistance of the microchannel. According to the Hagen–Poiseuille equation, the flow rate at $t = 0$ is governed by:

$$Q = \frac{\Delta P}{R_h} \tag{1}$$

where R_h is the hydraulic resistance of the microchannel. For a microchannel with rectangular cross-sections, the hydraulic resistance can be calculated as:

$$R_h = \frac{12\mu L}{h^3 w\left(1 - 0.63\frac{h}{w}\right)} \tag{2}$$

where μ is the dynamic viscosity of the culture medium, L, w and h correspond to the microchannel length, width, and height, respectively.

As fluid redistributes between the reservoirs, the liquid-level difference decreases, reducing the hydrostatic pressure over time. This leads to a transient flow regime in which the hydrostatic imbalance decays exponentially, following:[44,46]

$$\Delta h(t) = \Delta h_0 e^{-\frac{2\rho g}{A R_h} t} \tag{3}$$

where, A is the reservoir cross-sectional area. Consequently, both the instantaneous pressure drop and the flow rate $Q(t)$ decrease exponentially during the dwell period as the reservoir liquid levels gradually equilibrate.

2.2 Fluid dynamic simulation

Time-dependent simulations were performed in COMSOL Multiphysics (COMSOL, Inc.) to model hydrodynamic behavior within a single microfluidic unit under gravity-driven flow following previously described methods.[44,46] The laminar flow interface was employed to model with fluid parameters corresponding to DMEM culture medium at 37 °C (fluid density ρ = 1002 kg m^{-3}, dynamic viscosity $\mu = 0.861 \times 10^{-3}$ Pa s). Flow conditions were defined as: tilt angles α of 10° or 25°, dwell time of 300 s, and a rotation rate of 1 rpm, with the inlet reservoir fully filled and the outlet reservoir half-filled prior to rocker tilt. During the dwell period, the microfluidic chip was held at a fixed tilt angle α. Gravity was applied as a body force, with its vector components defined according to the horizontal and vertical directions of the microchannel at the imposed tilt, thereby generating the hydrostatic pressure component driving flow along the channel. All channel walls were assigned no-slip, impermeable boundary conditions. Considering $t = 0$ when the rocker plate achieved the tilt angle α, the initial reservoir heights were specified to impose the initial hydrostatic

imbalance Δh_0 and the exponential decay behavior of $\Delta h(t)$ was simulated during the dwell period. As in the previous study, to quantify mechanical stimuli within the microchannel, FSS was computed directly from the velocity gradients and FSS distribution at the bottom surface of the microchannels was visualized using color mapping and 1D profile plots at different channel widths over time (0–300 s dwell period).

2.3 Chip coating

To promote cell adhesion, microchannels were coated with extracellular matrix (ECM) proteins: human collagen type IV (C5533-5MG, BioReagent), fibronectin (Corning™, 356008), laminin-521 (Gibco™, A29248), or a mixture of fibronectin and collagen type IV. Coating solutions were prepared in DPBS at final concentrations of 100 μg mL^{-1} (fibronectin), 400 μg mL^{-1} (collagen IV), and 10 μg mL^{-1} (laminin). For the mixed coating, fibronectin and collagen IV were combined at 100 μg mL^{-1} and 400 μg mL^{-1}, respectively. Approximately 70 μL of coating solution was pipetted into one inlet to fill the microchannels without bubble formation. Chips were placed on an AKITA rocker plate (Finnadvance Ltd.) and incubated at 37 °C, 5% CO_2 for 4 h, oscillating between ±25° at 1 rpm with a 5 min dwell time. After incubation, coating solutions were replaced with pre-warmed human chondrocyte growth medium (HC Growth Medium, Cell Applications, 411-500).

2.4 Flow rate measurement

To quantify the gravity-driven flow rate during the dwell period at a rocker tilt angle of θ = 25°, microchannels were first coated with a mixture of fibronectin (100 μg mL^{-1}) and collagen IV (400 μg mL^{-1}) solution in DPBS for 4 h and then incubated with chondrocyte culture medium for 2 h at 37 °C and 5% CO_2. After preparation, the inlet reservoir was completely filled with culture medium, while the outlet reservoir was filled to half of its volume.

The microfluidic chip was placed on a rocker at room temperature, and t = 0 s was defined as the moment the rocker reached a tilt angle of 25°. At predetermined time points, the medium that had flowed into the outlet reservoir during each interval was removed and its volume determined by weighing the withdrawn fluid. Measurements were performed every 60 s over a total dwell duration of 300 s at the 25° tilt position. Flow-rate experiments were conducted on five independent microfluidic units.

An initial volume (V_0) was collected at t_0 = 0 s. The cumulative volume at each subsequent time point t_i was calculated by adding the amount transferred during that interval (V_i) to the cumulative volume from the previous time point. The instantaneous flow rate was then determined as the change in volume over each 60 s interval.

2.5 Cell culture and induced inflammation

Cryopreserved healthy human articular chondrocytes (Cell Applications, 402-05) were expanded from passage 2 to 5 in T75 and T175 flasks to obtain sufficient cells for five chips (24 units each). At confluency, cells were detached using 5 mL trypsin–EDTA (Sigma Aldrich, T3924) for 5 min, neutralized with 5 mL defined trypsin inhibitor (Cascade Biologics™, Gibco), and resuspended in pre-warmed chondrocyte medium at 2×10^6 cells per mL. For seeding, 35 μL of cell suspension was pipetted into the microchannels after removing medium from reservoirs (without emptying channels). Chips were inverted for 30 min to promote adhesion on the upper surface, then an additional 35 μL was added to the inlet and chips gently tilted for uniform distribution. Chips were maintained under static conditions for 24 h at 37 °C, 5% CO_2, followed by dynamic culture on AKITA rocker plates oscillating between ±25° at 1 rpm with 5 min dwell time. Medium was replaced daily until day 14 to support chondrocyte maturation and ECM deposition. From day 15 to day 21, IL-1β (R&D Systems, 201-LB-025) was added to the medium at 1 ng mL^{-1} or 10 ng mL^{-1} to induce an inflammatory phenotype. Medium was replaced daily during stimulation. Control samples received medium without cytokines. Cell culture on 2D surfaces: additional reference samples were prepared on 2D substrates. Glass slides bonded to PDMS gaskets and 48-well plates were coated with PDMS (crosslinker-to-base ratio 1 : 10) and cured at 65 °C for 4 h. Samples were cleaned with 96% ethanol, sterilized under UV light, and coated with 150 μL of the specified protein solution prior to cell seeding. For seeding, 20 μL of cell suspension (2×10^6 cells per mL) was added to each well, followed by 500 μL of culture medium. Samples were maintained under static conditions at 37 °C and 5% CO_2.

2.6 Assays and imaging

2.6.1 Cell metabolic activity. Cell metabolic activity was assessed at defined time points using PrestoBlue™ Cell Viability Reagent (A13261, Invitrogen). A working solution was prepared by mixing 90% pre-warmed chondrocyte culture medium with 10% reagent. After removing the medium from the reservoirs and rinsing the channels with warm DPBS, 150 μL of working solution was added to five culture units containing cells and three blank units per sample type. Chips were protected from light and incubated on an AKITA rocker at 37 °C, 5% CO_2 for 1 h. Following incubation, solutions were collected, mixed, and transferred to a black 384-well plate (40 μL per well). Five replicates per sample type were prepared in duplicate. Fluorescence was measured using a Victor Wallac microplate reader (excitation: 535 nm; emission: 615 nm). Duplicate readings were averaged and mean ± SD values were calculated from five replicates.

2.6.2 Live/dead staining. Cell viability was evaluated using the Live/Dead Viability/Cytotoxicity Kit (LS224, Invitrogen), containing calcein-AM (live cells, green) and ethidium homodimer-1 (EthD-1, dead cells, red). After removing medium from reservoirs (keeping channels filled), a working solution of 0.5 μM calcein-AM and 0.25 μM EthD-1 in warm culture medium was added. Chips were incubated on an AKITA rocker at 37 °C, 5% CO_2 for 30 min, then rinsed and imaged. Control samples were stained on days 3, 7, 14, and 21; IL-1β-stimulated samples (1 ng mL^{-1} and 10 ng mL^{-1}) were stained on day 21.

For each replicate, four images were acquired per region (I, II, III), totaling 12 images per region. Imaging was performed using a Leica DM4 wide-field fluorescence microscope (upright configuration, 10× objective) with filters for green (450–490 nm excitation/500–550 nm emission) and red (532–558 nm excitation/572–648 nm emission).

2.6.3 TRITC-phalloidin staining for F-actin visualization. Cell morphology was assessed on day 14 using TRITC-phalloidin staining (FAK100, Merck) in chips coated with collagen IV, fibronectin, or laminin. Three replicates per coating condition were prepared. After removing medium, cells were fixed with 4% paraformaldehyde in DPBS for 15 min at RT, washed three times with DPBS (200 μL per unit), and incubated overnight at 4 °C in blocking solution (10% NDS, 1% BSA, 0.1% Triton X-100 in DPBS). Samples were then incubated for 2 h at RT with staining solution (TRITC-phalloidin 1 : 800 in DPBS with 1% BSA), washed, and counterstained with DAPI (1 : 2000 in DPBS). All steps were performed on an AKITA rocker. Imaging was conducted using a Leica DM6 Thunder fluorescence microscope (upright configuration, motorized stage) with tile scans and z-stacks processed using Thunder deconvolution. TRITC-phalloidin was imaged using filters (532–558 nm excitation/572–648 nm emission) and DAPI using 382–408 nm excitation/435–485 nm emission with a 40× objective.

2.6.4 Immunofluorescence analysis for collagen type II and aggrecan. Cells were fixed with 4% paraformaldehyde (PFA) following the same protocol as F-actin staining. Control samples were fixed on days 3, 7, 14, and 21; IL-1β-stimulated samples (1 ng mL^{-1} and 10 ng mL^{-1}) were fixed on day 21. All samples were stained simultaneously. Fixed samples were washed twice with DPBS (5 min each) and incubated for 1 h at room temperature (RT) in blocking solution (10% NDS, 1% BSA, 0.1% Triton X-100 in DPBS). Primary antibodies collagen type II (NB600-844, Novus Biologicals) and aggrecan (AF1220, R&D Systems) were diluted in blocking solution to 1 : 200 and 5 μg mL^{-1}, respectively. Approximately 70 μL of antibody solution was added to each unit, and chips were incubated overnight at 4 °C on a rocker. After incubation, samples were washed four times with DPBS (2 min each) and incubated for 2 h at RT with secondary antibodies diluted 1 : 200 in blocking solution: rabbit anti-mouse (NB7543, Novus Biologicals) for collagen II and donkey anti-goat (NL557, R&D Systems) for aggrecan. Samples were protected from light during incubation. Following four DPBS washes, nuclei were counterstained with DAPI (1 : 2000 in DPBS) for 5 min, washed once, and reservoirs filled with DPBS. All steps were performed on an AKITA rocker. Imaging was conducted using a Leica DM6 Thunder wide-field fluorescence microscope (upright configuration, 20× objective) with filters for collagen II (green: 450–490 nm excitation/500–550 nm emission), aggrecan (red: 532–558 nm excitation/572–648 nm emission), and DAPI (blue: 382–408 nm excitation/435–485 nm emission). Images were acquired as z-stacks from the bottom to the top of the microfluidic channels, and final images are presented as z-projections of the acquired slices.

2.6.5 Image quantification. Immunofluorescence images were analyzed using Fiji (ImageJ). Z-stacks were split into three channels corresponding to collagen II (green), aggrecan (red), and DAPI (blue). Quantification was performed on slices corresponding to the base of the microchannel. Regions of interest (ROIs) were manually drawn around individual cells in the green channel (collagen II), and the same ROIs were then applied to the red channel (aggrecan). Only well-isolated cells were selected; cells that appeared blurred, out of focus, or embedded within aggregates were excluded (Fig. S1). For each image, five background ROIs (100 × 100 μm) were measured, and the mean background intensity was used for correction. Integrated density was obtained for each cell, and corrected total cell fluorescence (CTCF) was calculated as: CTCF = integrated density − (cell area × mean background intensity).

CTCF values from the green channel quantified collagen II expression; the same ROIs were applied to the red channel for aggrecan CTCF quantification. For time-course analysis (days 3, 7, 14, 21), 41 cells per region were analyzed across three control samples per time point. For IL-1β stimulation (day 21), 44 cells per region were analyzed for control and cytokine-treated samples (1 ng mL^{-1} and 10 ng mL^{-1}).

2.6.6 ELISA assays. Inflammatory markers released into the culture medium were quantified using chemiluminescent multiplex ELISA. For each sample type (control and IL-1β-stimulated at 1 ng mL^{-1} and 10 ng mL^{-1}), 150 μL of medium was collected from chip reservoirs, centrifuged to remove particulates, and stored at −20 °C or 4 °C prior to analysis. Matrix metalloproteinases (MMP-1, MMP-2, MMP-3, MMP-7, MMP-9, MMP-13) were measured using Q-Plex™ Human MMP 6-Plex (340949HU, Quansys Biosciences), and cytokines (IL-1β, IL-6, IL-8, TNF-α) using Q-Plex™ Human Custom 4-Plex (107749GR, Quansys Biosciences). Three biological replicates per condition and three blanks were analyzed in duplicate. Samples were diluted at 1 : 2, 1 : 100, and 1 : 1000 to ensure values fell within the assay detection range. Assays were performed according to manufacturer protocols. Plates were imaged using Q-Viewer Imager LS (Quansys Biosciences) with 270 s exposure. Chemiluminescence intensities were processed by averaging duplicates, subtracting background, and fitting calibration curves using a four-parameter logistic model in Origin software to calculate concentrations. Data is reported as mean ± SD for three replicates per condition. Measurements below the detection limit were indicated as <LLOQ (lower limit of quantification). Additionally, collagen type II released into the medium was quantified using human collagen type II alpha 1 (COL2A1) ELISA kit (BSKH63293, Bioss Antibodies). Samples collected on day 21 were processed as above, loaded into pre-coated 96-well plates (100 μL per well), and analyzed per manufacturer instructions. Absorbance was measured at 450 nm using Absorbance 96 (Byonoy). Concentrations were calculated using calibration curves fitted in Origin software and reported as mean ± SD for three replicates per condition.

2.7 Statistical analysis

Statistical analysis was performed using the non-parametric Kruskal–Wallis test followed by Dunn's *post hoc* test for multiple comparisons (Origin software). Differences were considered significant at $p < 0.05$. Significance levels are indicated as follows: $p < 0.05$ (*), $p < 0.01$ (**), $p < 0.001$ (***), and $p < 0.0001$ (****); "n.s." denotes non-significant differences.

3. Results

3.1 Optimization of microfluidic chips configuration for human articular chondrocytes

To establish conditions for long-term chondrocyte culture in the microfluidic platform, we first optimized extracellular matrix (ECM) coatings under a stable gravity-driven flow regime (rocker tilt: 25°). Given the critical role of ECM coatings in cell adhesion and proliferation three ECM components were evaluated: collagen type IV, fibronectin, and laminin-521.

Fluorescence imaging of F-actin (Fig. 2A) revealed that fibronectin-coated channels supported higher cell density and a rounded morphology in regions I and II of the microchannels, closely resembling native chondrocyte phenotype and 3D culture morphology. In contrast, cells in region III appeared more elongated across all coatings, likely due to higher FSS.

Cell metabolic activity was assessed using PrestoBlue™ on days 3, 7, and 14 (Fig. 2B). Laminin-coated samples exhibited significantly higher metabolic activity than collagen type IV and comparable levels to fibronectin. Additionally, F-actin imaging indicated that laminin promoted cytoskeletal spreading rather than rounded morphology. Laminin and collagen coatings showed lower cell density, possibly due to non-uniform adsorption. Collagen type IV supported aggregate formation and rounded cells, suggesting suitability for chondrocyte culture, though adhesion could be improved. To enhance chondrocytes viability and adhesion within the channels, a mixed coating of fibronectin and collagen type IV was tested. Metabolic activity was significantly higher for the mixture compared to fibronectin alone up to day 21 (Fig. 2C), correlating with greater cell coverage observed in live/dead imaging on day 14 (Fig. S2). F-actin staining on day 21 confirmed robust cultures with 3D aggregates and microtissue-like structures across all channel regions (Fig. S3, Videos S1–S3). Despite the differences in cell behavior observed between the tested coatings in microchannels, no significant differences were observed among coatings in 2D PDMS-coated glass controls. Live/dead images acquired on

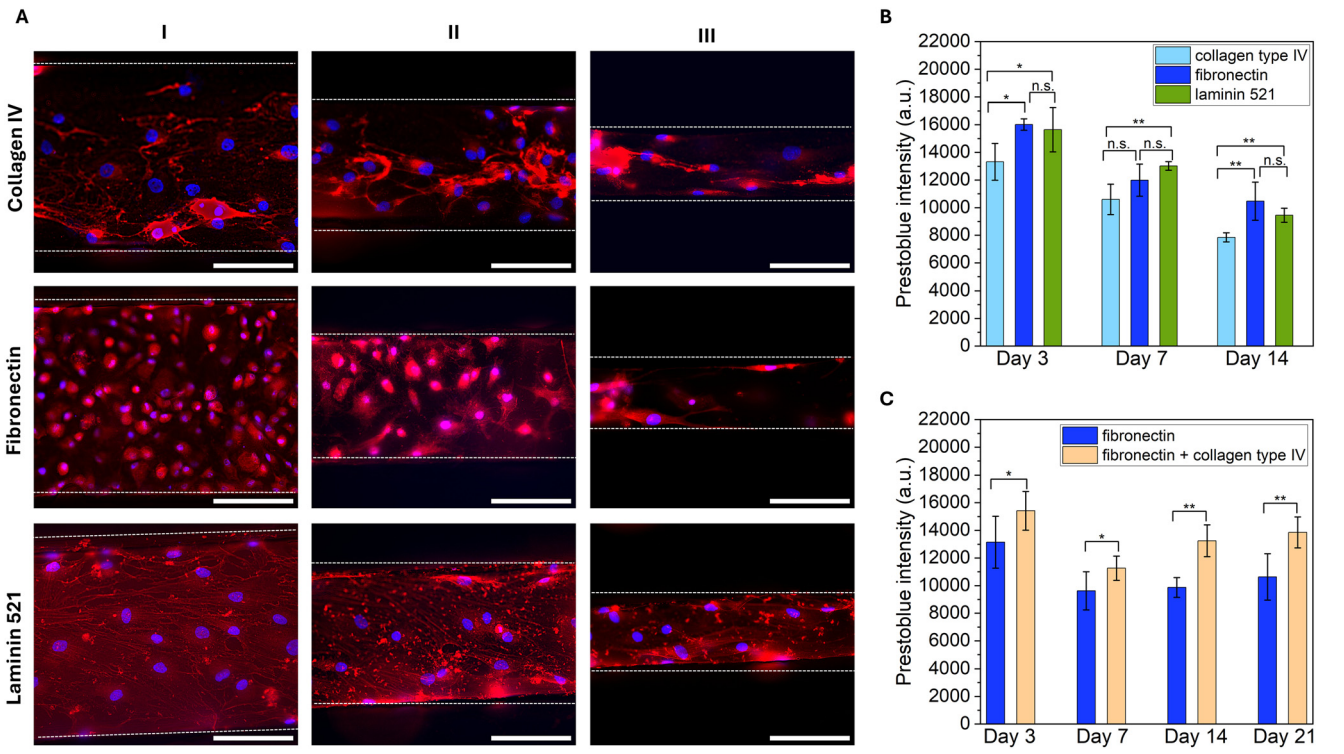

Fig. 2 Optimization of ECM coating for chondrocyte culture in a microfluidic environment. A rocker tilt angle of θ = 25° was applied to generate gravity-driven flow. (A) Representative wide-field fluorescence images of F-actin (red) and nuclei (blue) from chondrocytes cultured for 14 days in microchannels coated with different ECM proteins, shown across regions I–III. Scale bar = 100 μm. White dashed lines indicate microchannel boundaries in all fluorescence images. (B and C) Cell metabolic activity measured by PrestoBlue™ assay at multiple time points. (B) Comparison across individual ECM coatings up to day 14. (C) Comparison between fibronectin alone and a fibronectin–collagen IV mixture up to day 21. N = 5 independent samples per group. Statistical analysis: Kruskal–Wallis with Dunn's *post hoc* test; $p < 0.05$ (*), $p < 0.01$ (**).

day 21 presented comparable cell viability and proliferation in 2D PDMS-coated samples for both fibronectin and fibronectin–collagen type IV mixture (Fig. S4A). Cell metabolic activity also showed comparable results between different coatings (Fig. S4B and C) although a slight increase of approximately 10% was noted for the mixed coating on day 21 (Fig. S4C).

Overall, the fibronectin–collagen type IV mixture provided superior adhesion and proliferation in the microchannels, as supported by imaging and metabolic assays. This coating was therefore selected for all subsequent experiments to model healthy chondrocytes and induced inflammation.

We next examined whether FSS magnitude affected chondrocyte behavior by comparing two rocker tilt angles (θ

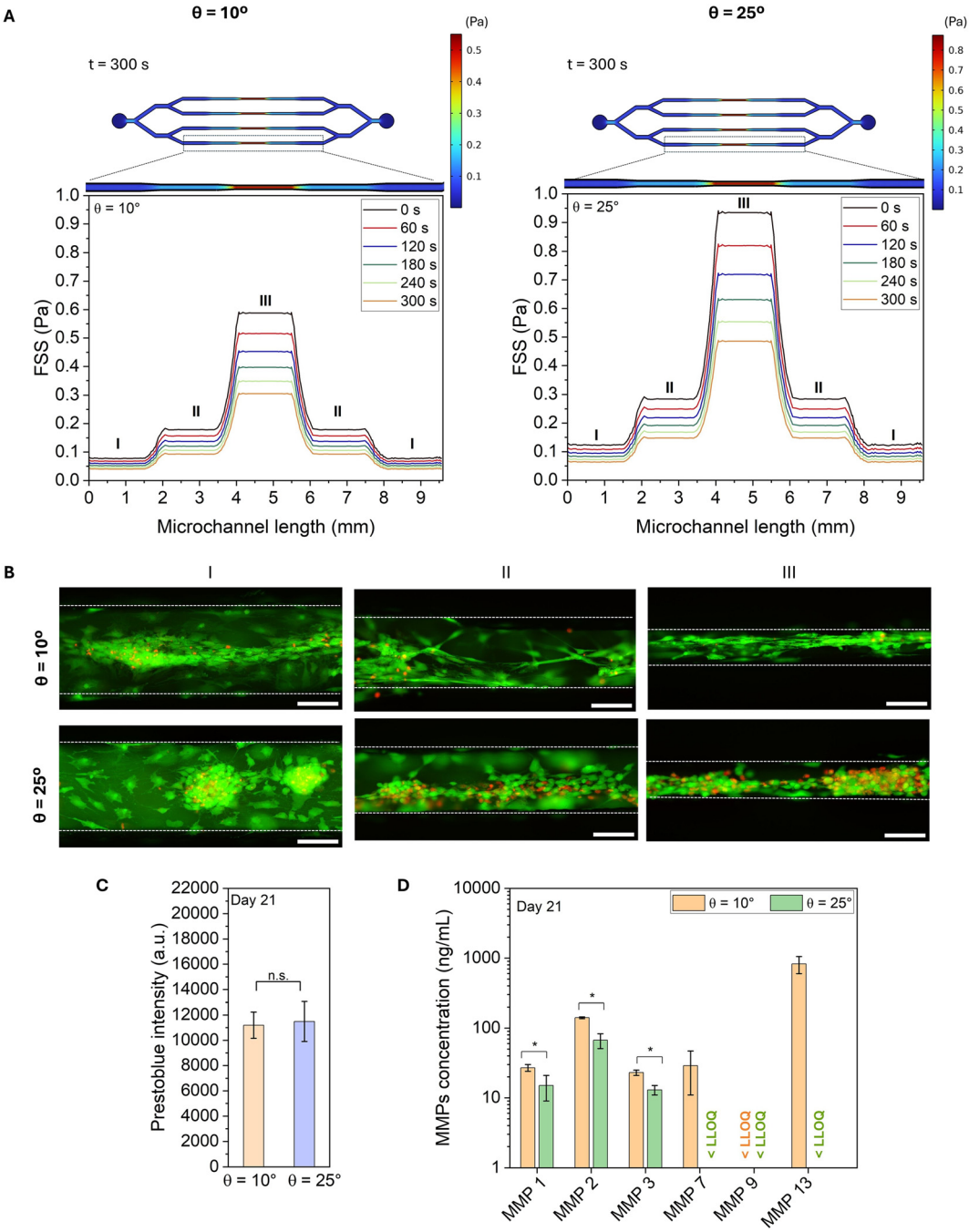

Fig. 3 (A) COMSOL simulations of FSS at the bottom surface of the microchannels for rocker tilt angles θ = 10° and θ = 25°. Top: Color map of FSS distribution along microchannel length; bottom: FSS profiles over time (0–300 s dwell period). (B) live/dead images on day 21 for θ = 10° and θ = 25° across regions I–III. White dashed lines indicate microchannel boundaries in all fluorescence images. (C) Cell metabolic activity on day 21 for θ = 10° and θ = 25°. N = 5 independent samples per group. (D) Concentrations of MMPs secreted on day 21 measured by Q-Plex™ ELISA for θ = 10° and θ = 25°. N = 3 independent samples per group. <LLOQ indicates values below the lower limit of quantification. Statistical analysis: Kruskal–Wallis with Dunn's *post hoc* test; $p < 0.05$ (*).

= 10° and θ = 25°). In this gravity-driven system, tilt angle determines pressure differences between reservoirs, thereby modulating flow rate and FSS. COMSOL simulations predicted FSS distribution along microchannel walls for regions I–III at both tilt angles. FSS increased progressively from region I (low) to region III (high) and remained uniform within each region. Increasing tilt from 10° to 25° elevated FSS, with maximum values of 0.6 Pa and 0.9 Pa in region III for θ = 10° and θ = 25°, respectively (Fig. 3A). Simulations also revealed temporal variation in FSS during the 300 s dwell period, as medium height changed over time. To experimentally characterize these dynamics at the 25° condition, we quantified the volume of medium transferred to the outlet reservoir at four time points measured every 60 s during the dwell period (Fig. S5A) and calculated the corresponding instantaneous flow rates based on the 60 s volume increments (Fig. S5B). The cumulative volume increased linearly while the instantaneous flow rate exhibited a pronounced peak during the first interval, followed by a rapid decline and stabilization at lower values. This pattern is consistent with the transient nature of gravity-driven flow, where the hydrostatic pressure difference is highest immediately after the platform reaches the target tilt angle and decreases as reservoir fluid levels equilibrate.

To evaluate the impact of these flow regimes on cell behavior, experimental validation was performed by culturing chondrocytes for 21 days under both tilt conditions. live/dead staining (Fig. 3B) and PrestoBlue™ metabolic activity assays (Fig. 3C) confirmed high viability for both angles. ELISA analysis on day 21 showed significantly higher secretion of catabolic MMPs (MMP-1, MMP-2, MMP-3, MMP-7, MMP-9) at 10° compared to 25° (Fig. 3D). Of note, static (no-flow) cultures rapidly lost viability (data not shown), emphasizing the necessity of dynamic perfusion. Based on these findings, subsequent experiments were conducted at 25°, which preserved viability while minimizing catabolic responses, providing physiologically relevant FSS for long-term culture.

3.2 Validation of healthy human articular chondrocytes cell culture overtime under various magnitudes of fluid shear stress

To validate the optimized microfluidic chip, we assessed viability, proliferation, and matrix marker expression over 21 days. Live/dead staining confirmed sustained high viability across all regions (Fig. 4A–C). Cell numbers increased progressively, accompanied by the formation of 3D aggregates and contracted microtissue-like structures, particularly evident at later time points.

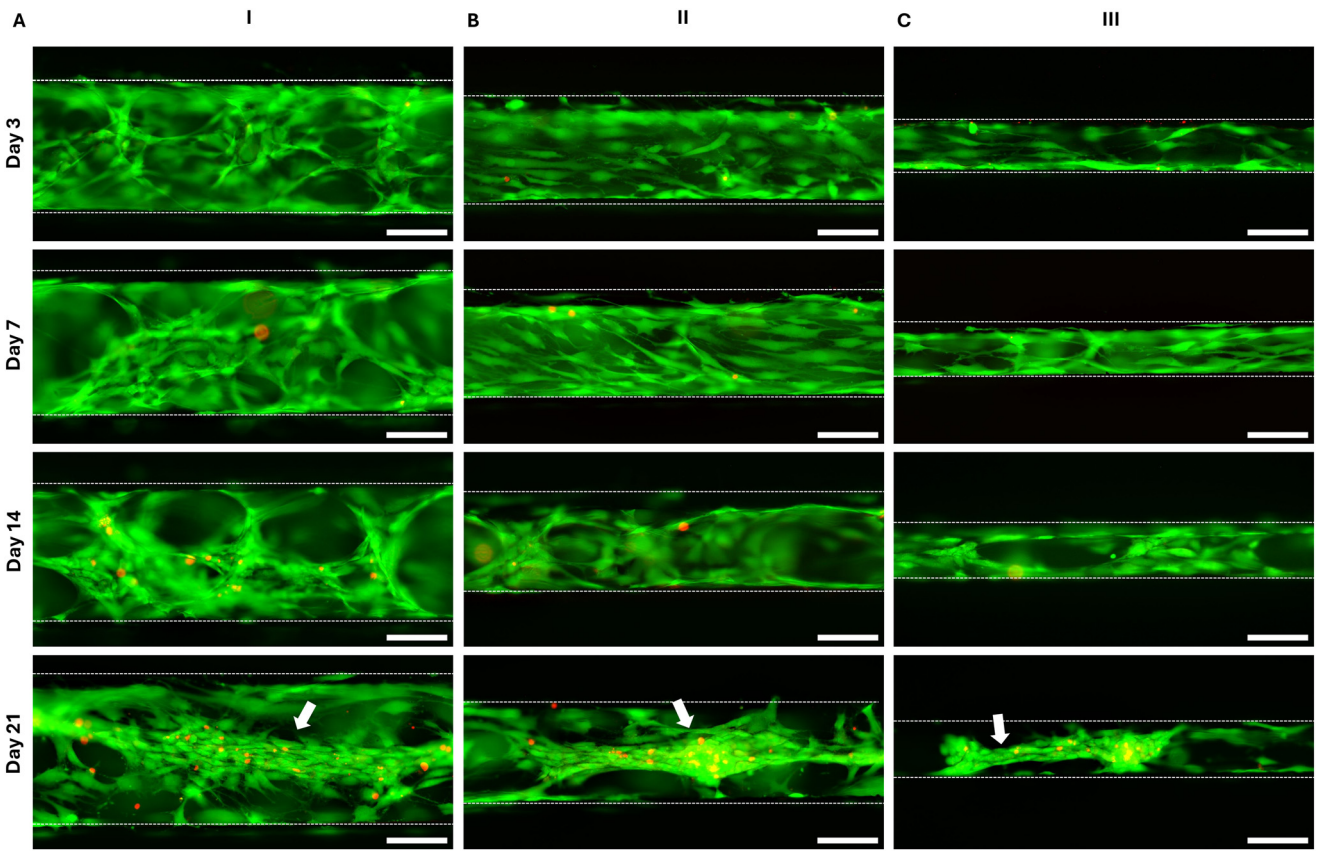

Fig. 4 Long-term viability and proliferation of chondrocytes under varying FSS. Wide-field fluorescence images of live/dead staining at days 3, 7, 14, and 21 for (A) region I (low FSS), (B) region II (medium FSS), and (C) region III (high FSS). Cells remain viable throughout culture, with contracted microtissue-like structures evident by day 21 (white arrows), even in regions exposed to higher FSS. Green: calcein-AM (live); red: EthD-1 (dead). White dashed lines indicate microchannel boundaries. Scale bar: 100 μm.

Morphological differences were observed across regions: cells in region I (low FSS) exhibited random orientation and partial alignment with flow, whereas cells in regions II and III were predominantly elongated along the flow direction, except within aggregates. TRITC-phalloidin staining on day 21 corroborated these observations, revealing actin filament organization consistent with FSS-induced alignment (Fig. S3).

To assess extracellular matrix (ECM) synthesis, immunofluorescence analysis was performed at days 3, 7, 14, and 21 to quantify collagen type II, the primary collagen in articular cartilage, and aggrecan, the major cartilage proteoglycan (Fig. 5). Collagen type II expression was low at day 3 but increased markedly by day 7 in regions I and II, with further elevation across all regions at days 14 and 21. Furthermore, collagen type II expression on day 21 is higher in region I, suggesting that lower FSS is preferrable for ECM establishment. In contrast, aggrecan expression was high on day 3, showed a modest increase by day 7, and gradually declined thereafter.

Imaging revealed progressive formation of cell aggregates and microtissue-like structures over time, consistent with observations from live/dead and F-actin staining. Collectively, sustained viability and increased collagen type II and aggrecan expression confirm the suitability of this microfluidic model for studying chondrocyte proliferation and cartilage-specific ECM production under varying FSS conditions.

3.3 Inflammatory response model induced by IL-1β under FSS

The optimized microfluidic model was used to investigate the effects of the pro-inflammatory cytokine IL-1β on chondrocyte viability, metabolic activity, ECM integrity, and catabolic factor secretion under dynamic flow. Healthy chondrocytes were cultured for 14 days to allow proliferation

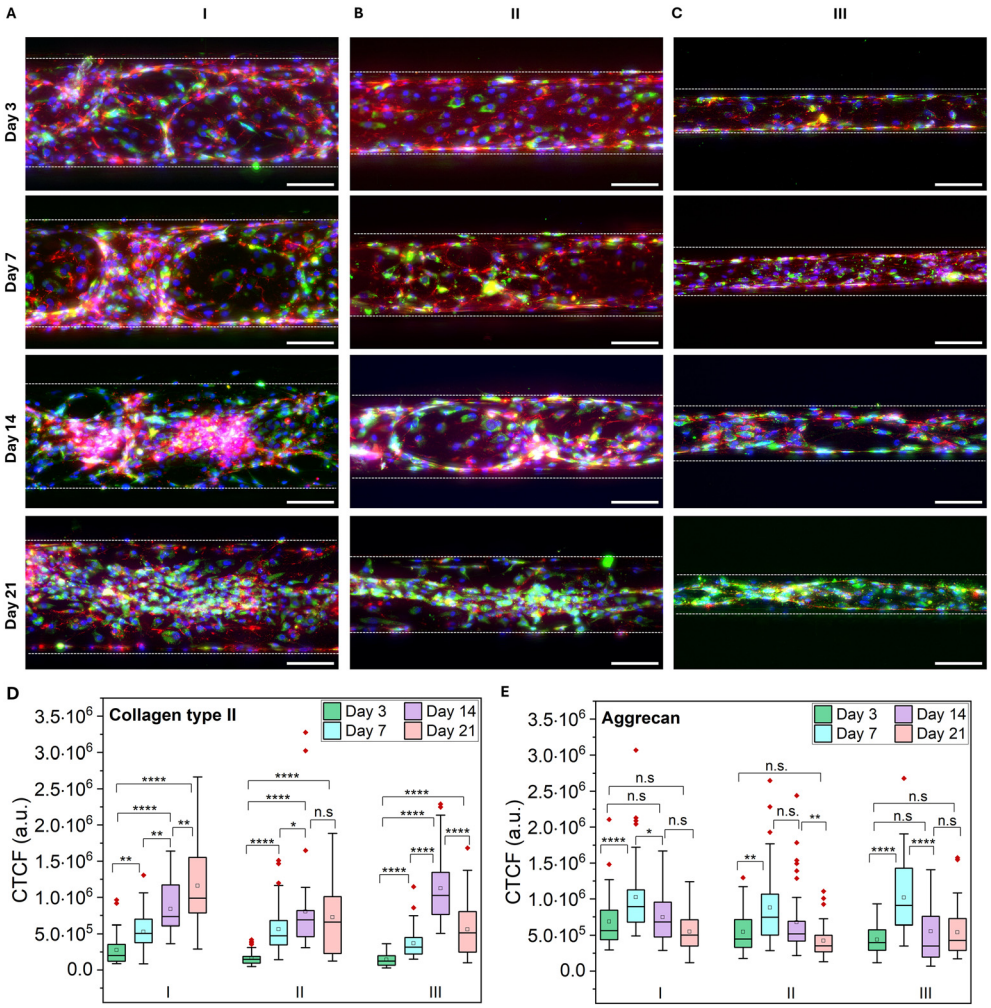

Fig. 5 Expression of extracellular matrix (ECM) markers under healthy conditions. (A–C) Wide-field immunofluorescence images of chondrocytes cultured under varying FSS at days 3, 7, 14, and 21: (A) region I (low FSS), (B) region II (medium FSS), and (C) region III (high FSS). Collagen type II (green) and aggrecan (red) are shown with nuclei (DAPI, blue). Images represent 3D projections of z-stacks acquired from the bottom to the top of the microchannels. Scale bar = 100 μm. (D and E) Quantification of collagen type II and aggrecan expression over time in regions I–III using corrected total cell fluorescence (CTCF) (n = 41 cells per group). Statistical analysis: Kruskal–Wallis test with Dunn's *post hoc* comparison; significance indicated as ****$p < 0.0001$, **$p < 0.01$, *$p < 0.05$; n.s. = non-significant.

and ECM maturation, followed by exposure to IL-1β (1 ng mL^{-1} or 10 ng mL^{-1}) for 7 days. Live/dead staining on day 21 revealed no significant increase in cell death in IL-1β-treated samples compared to controls (Fig. 6A–C). However, imaging showed disruption of cell aggregates across all channel regions in IL-1β-stimulated samples, suggesting ECM degradation. This observation aligns with the known role of IL-1β in promoting collagen fibril breakdown within cartilage matrix. In 2D static cultures on PDMS-coated surfaces, control samples appeared confluent by day 21, covering nearly the entire surface. Similar to observations in our microfluidic platform, IL-1β stimulation at 1 ng mL^{-1} and 10 ng mL^{-1} did not compromise cell viability on 2D surfaces (Fig. S6A). Although live/dead imaging revealed increased intercellular spaces in cytokine-stimulated 2D cultures, the phenotypic effects of IL-1β were more pronounced in the microfluidic system.

To confirm cell viability under inflammatory conditions, metabolic activity was assessed using PrestoBlue™ for control and IL-1β-stimulated samples. A modest increase of approximately 9.5% was observed following exposure to 1 ng mL^{-1} IL-1β, while a significant rise of 28.5% was detected at

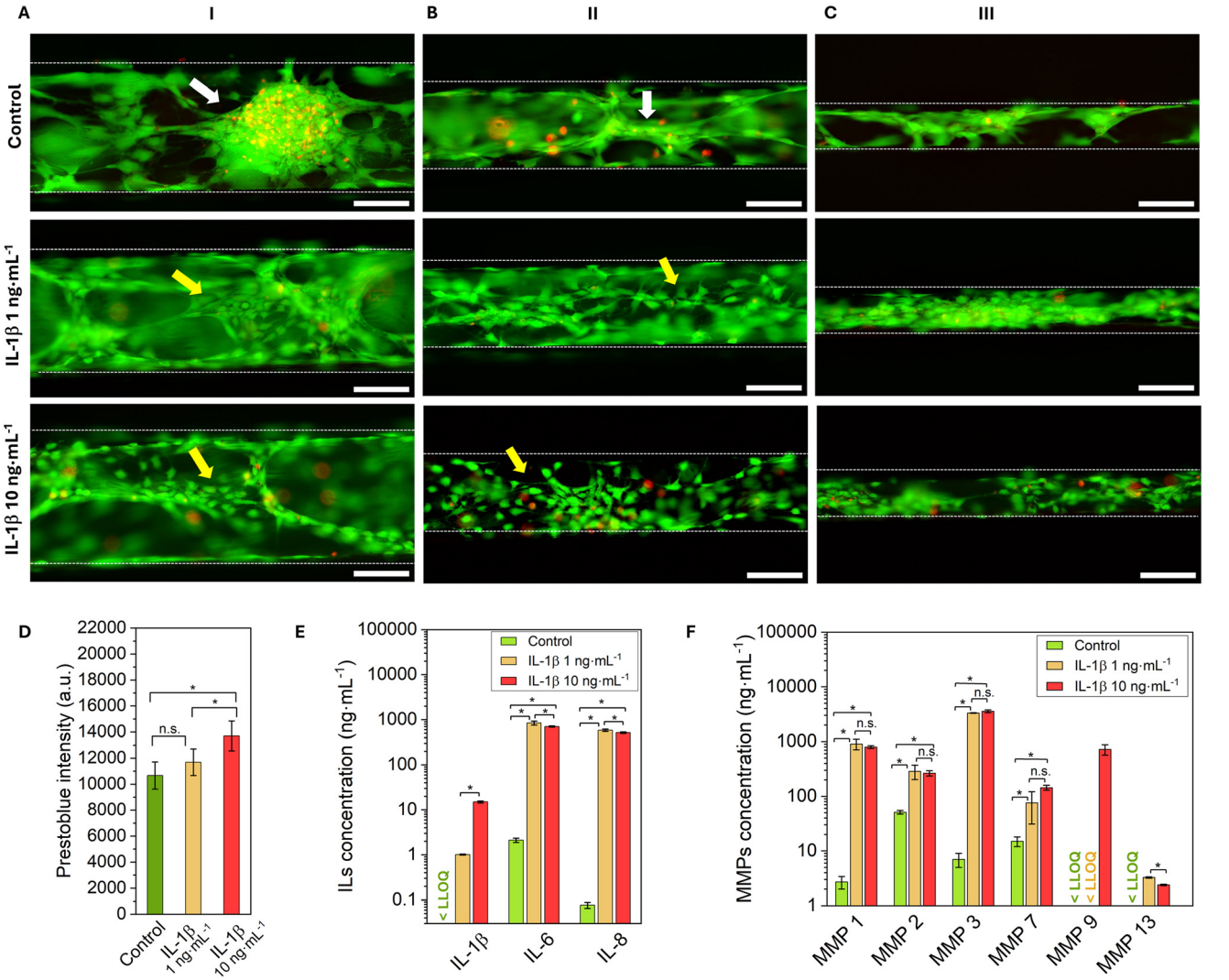

Fig. 6 Cell viability, metabolic activity, and secretion of catabolic markers under healthy and IL-1β-induced inflammatory conditions. (A–C) Representative wide-field fluorescence images of human articular chondrocytes cultured in microchannels under dynamic flow, stained with live/dead on day 21. Conditions include control (no cytokine) and IL-1β stimulation (1 ng mL^{-1} and 10 ng mL^{-1} from day 15 to day 21). Images were acquired on day 21 from (A) region I (low FSS), (B) region II (medium FSS), and (C) region III (high FSS). Dense cell aggregates in control samples are indicated with white arrows in regions I and II, and disrupted aggregates in IL-1β-stimulated samples are indicated with yellow arrows. (D) Cell metabolic activity measured by PrestoBlue™ assay for control samples at multiple time points and IL-1β-stimulated samples on day 21 (1 ng mL^{-1} and 10 ng mL^{-1}). N = 5 independent samples per group. Statistical analysis: Kruskal–Wallis with Dunn's *post hoc* test; $p < 0.05$ (*), n.s. = non-significant. (E and F) Quantification of inflammatory markers in culture medium collected on day 21 using multiplex ELISA: (E) MMPs (MMP-1, MMP-2, MMP-3, MMP-7, MMP-9, MMP-13) and (F) cytokines (IL-1β, IL-6, IL-8). Healthy chondrocytes were cultured for 14 days before IL-1β stimulation for 7 days. N = 3 independent samples per group, measured in duplicate. <LLOQ indicates values below the lower limit of quantification. Statistical analysis: Kruskal–Wallis with Dunn's *post hoc* test; $p < 0.05$ (*), n.s. = non-significant.

10 ng mL^{-1} compared to the control (Fig. 6D). In contrast to microchannels, 2D stimulated samples exhibited reduced metabolic activity compared to controls (Fig. S6B and C).

To further characterize the inflammatory response, secretion of interleukins (IL-1β, IL-6, IL-8) and matrix metalloproteinases (MMP-1, MMP-2, MMP-3, MMP-7, MMP-9, MMP-13) was quantified using multiplex ELISA (Fig. 6E and F). All markers were significantly elevated in stimulated samples compared to controls. Notably, measured IL-1β levels reflect both exogenous cytokine and cell-derived production. MMPs and interleukins detected here are key mediators of cartilage degradation, with MMP-13 strongly associated with collagen type II breakdown in osteoarthritis. Overall, the tested IL-1β concentrations provided comparable inflammatory response (Fig. 6E and F). Collagen type II degradation fragments in culture medium were also quantified by ELISA (Fig. S7), confirming significantly higher levels in IL-1β-stimulated samples *versus* controls, consistent with ECM degradation.

Immunofluorescence analysis on day 21 revealed disruption of microtissue-like structures in IL-1β-treated samples compared to controls (Fig. 7A–C), with visibly reduced fluorescence intensity for collagen type II and aggrecan. Quantitative analysis of corrected total cell fluorescence (CTCF) confirmed decreased expression of both markers upon IL-1β stimulation across all regions. For collagen type II, differences were significant between control and 10 ng mL^{-1} in region I, and between control and both IL-1β concentrations in regions II and III (Fig. 7D). Aggrecan expression showed significant reductions for stimulated samples in regions I and II, and for 10 ng mL^{-1} in region III (Fig. 7E).

Overall, IL-1β stimulation induced a catabolic phenotype characterized by increased secretion of inflammatory mediators, ECM degradation, and reduced expression of cartilage-specific markers, validating the microfluidic model for osteoarthritis-like conditions under physiologically relevant FSS.

4. Discussion

By leveraging and optimizing a streamlined 24-unit microfluidic platform, we achieved high-throughput experimentation, high reproducibility, and seamless

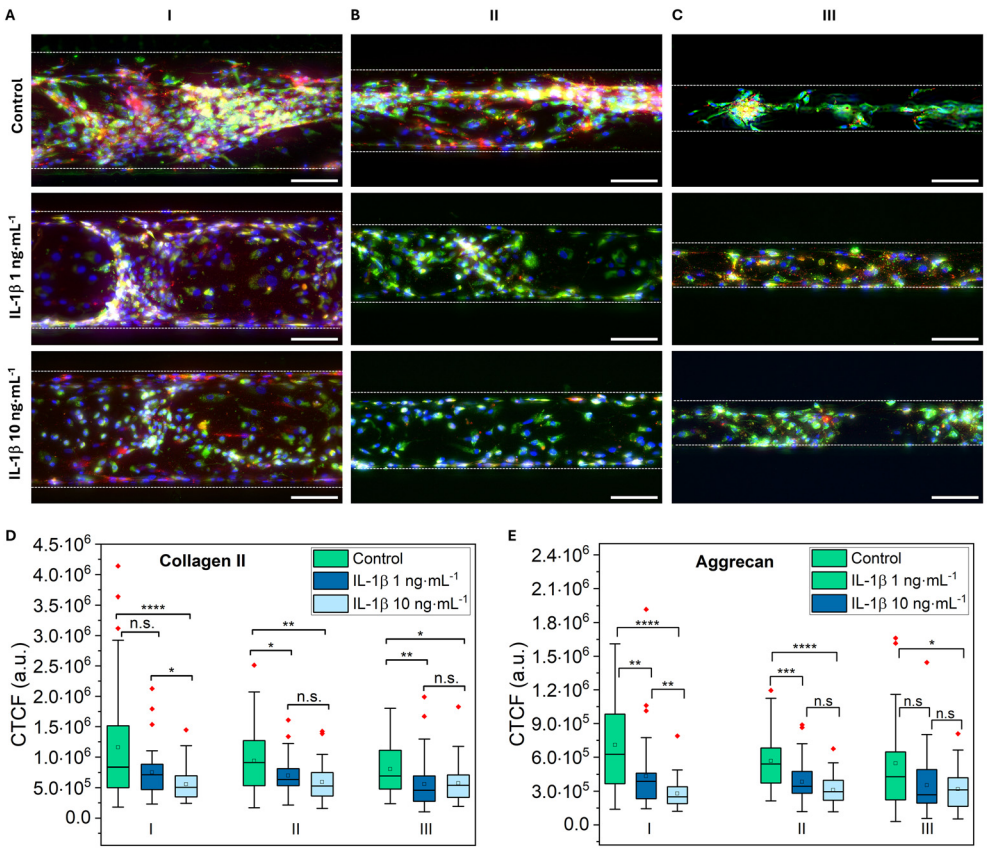

Fig. 7 Expression of extracellular matrix (ECM) markers under inflammatory conditions. (A–C) Representative wide-field immunofluorescence images of control and IL-1β-stimulated chondrocytes. Cells were cultured for 14 days, then stimulated with IL-1β (1 ng mL^{-1} or 10 ng mL^{-1}) for 7 days. Images were acquired on day 21 from (A) region I (low FSS), (B) region II (medium FSS), and (C) region III (high FSS). Channels: collagen type II (green), aggrecan (red), nuclei (DAPI, blue). Scale bar: 100 μm. (D and E) Quantification of collagen type II and aggrecan expression using corrected total cell fluorescence (CTCF). N = 44 cells per group. Statistical analysis: Kruskal–Wallis test with Dunn's *post hoc* comparison; significance indicated as ****$p < 0.0001$, ***$p < 0.001$, **$p < 0.01$, *$p < 0.05$; n.s. = non-significant.

integration into standard laboratory workflows, while fostering sustainable OoC development. The optimized microfluidic platform was validated for long-term culture of human articular chondrocytes and modeling of inflammatory responses under controlled FSS.

The microfluidic chips incorporate 24 culture units with microchannels of varying widths to generate spatial FSS gradients (regions I–III: low, medium, high FSS). This system mimics mechanical stimulation from interstitial fluid flow in cartilage, providing a physiologically relevant microenvironment compared to conventional 2D *in vitro* models. Even the highest FSS applied here (<1 Pa) remained within the range considered beneficial for chondrocytes, as previous studies[43,48] report that FSS below 2 Pa promotes proliferation and ECM synthesis, whereas excessive FSS (10–15 Pa) induces ECM degradation, apoptosis, and inflammation. Recent work by Zhao *et al.* demonstrated that low FSS (≈1.8 Pa) enhances chondrocyte proliferation and ECM production *via* ERK5/KLF4 signaling, highlighting the importance of mechanical cues in cartilage homeostasis.[48] Our approach extends these findings by applying controlled FSS gradients within a microfluidic device, enabling simultaneous evaluation of multiple shear conditions in a single high-throughput platform.

Coating optimization using ECM proteins revealed significant effects on chondrocyte adhesion, morphology, and metabolic activity. Among fibronectin, collagen type IV, laminin-521, and their combinations, a fibronectin–collagen IV mixture provided superior performance, supporting robust adhesion, proliferation, and formation of 3D aggregates. These observations align with the known roles of fibronectin in promoting chondrogenic differentiation, cell adhesion to surfaces and preventing apoptosis, and of collagen IV and laminin in pericellular matrix organization and mechanotransduction.[49–51] Importantly, collagen type II was not used as a coating to allow its endogenous production to be monitored.

Long-term culture validation demonstrated sustained cell viability, increased metabolic activity, and progressive extracellular matrix (ECM) deposition, as evidenced by collagen type II and aggrecan expression. Furthermore, the microfluidic chips facilitated the formation of three-dimensional cell aggregates and contracted microtissue-like structures, which were visualized using wide-field fluorescence microscopy. These structures closely resemble findings reported by Roehm *et al.*, where hMSCs differentiated within microchannels into chondrogenic phenotypes and formed thin, contracted cartilage-like structures after two weeks of chondrogenesis.[52]

Finally, we established an inflammatory model by stimulating mature chondrocytes with IL-1β (1 ng mL^{-1} and 10 ng mL^{-1}) for 7 days. While viability remained unaffected, IL-1β disrupted cell aggregates and reduced anabolic markers (collagen II, aggrecan), indicating ECM degradation. Conversely, catabolic responses were evident, with elevated secretion of MMPs (MMP-1, -2, -3, -7, -9, -13) and pro-inflammatory cytokines (IL-1β, IL-6, IL-8), consistent with osteoarthritic pathology. These findings confirm that the platform enables controlled induction of OA-like phenotypes under dynamic flow, offering a versatile tool for mechanobiology studies and therapeutic screening. Our results are consistent with previous work by Lin *et al.*, who demonstrated increased release of MMPs in a bioreactor system upon IL-1β stimulation (10 ng mL^{-1}).[53] Furthermore, given that in our work IL-1β stimulation at 1 ng mL^{-1} induced significant catabolic marker secretion, cytokine concentrations could be reduced in subsequent studies to avoid excessive inflammatory signaling.

It is important to highlight that while fluorescence imaging allowed us to evaluate cellular responses separately within each of the three shear-stress regions, the ELISA measurements were performed on pooled medium collected from the common outlet reservoir. As the outflow integrates secreted factors from regions I, II, and III, the resulting cytokine and MMP levels represent the overall inflammatory response of the entire channel rather than region-specific biochemical outputs.

In this study, we focused on low, physiologically supportive FSS to preserve chondrocyte health and used IL-1β stimulation to induce OA-like phenotypes, demonstrating the platform's suitability for high-throughput inflammation studies. These findings establish the foundation for future work to investigate the effects of hyperphysiological FSS as a direct mechanoinflammatory stimulus. In such studies, a mature, ECM-rich chondrocyte culture would first be generated under the beneficial FSS conditions defined here, after which overload-level shear stresses could be introduced to induce OA-like phenotypes without relying on cytokine stimulation. In addition, future studies will also benefit from measuring flow rate and shear stress after extended culture periods, as the formation of cell aggregates can alter hydraulic resistance within the microchannel and thereby lead to deviations between expected and actual shear conditions experienced by the cells.

Although highly relevant for high-throughput OA-related studies at the onset of inflammation, further device complexity, such as incorporating hydrogels or scaffolds for 3D growth and applying compressive forces, will be essential to mimic the physiological environment of osteoarthritic cartilage. Future work should also include adapted designs for modelling different joint tissues and enabling multi-tissue crosstalk, which is crucial for studying OA pathogenesis, as the disease affects the entire joint rather than cartilage alone. Several models already incorporate interfaces for joint tissue communication.[28,52,54–60] A recent study by Mainardi *et al.* developed a dual-compartment OoC platform to replicate OA crosstalk between bone and cartilage.[60] By engineering a vascularized osteochondral construct, they demonstrated that IL-1β exposure (1 ng mL^{-1}) promoted endothelial and stromal invasion into the cartilage layer, mimicking OA-associated inflammation.[60]

In summary, the microfluidic platform developed in this study provides a high-throughput and reproducible system for investigating chondrocyte inflammatory responses. While drug-testing experiments were not performed here, the platform's design and consistent induction of inflammation establish a strong foundation for future high-throughput screening of disease-modifying osteoarthritis drugs (DMOADs), particularly those aimed at inhibiting catabolic pathways and restoring anabolic activity to support cartilage repair. Despite the current configuration not incorporating a 3D extracellular matrix or mechanical compression, it offers several practical advantages, including efficient generation of large sample numbers, straightforward monitoring of cell behavior and ECM production using standard fluorescence microscopy, and simplified operation enabled by gravity-driven flow without external pumps or tubing Compared with conventional 2D cytokine-based models, this system provides distinct benefits, including (i) a microenvironment that supports cell–cell interactions and aggregate formation, (ii) mechanical stimulation through controlled FSS gradients, and (iii) reduced consumption of cells, medium, and reagents.

5. Conclusions

We exploited and optimized a high-throughput microfluidic platform for dynamic long-term culture of healthy human articular chondrocytes and induction of OA-like phenotypes through IL-1β stimulation. The chip design incorporates microchannels with varying widths to generate controlled FSS gradients, a key mechanical cue in cartilage physiology, and applies this model for the first time to human articular chondrocytes. The healthy chondrocyte model was validated by sustained viability, progressive ECM deposition (collagen type II and aggrecan), and formation of 3D aggregates and microtissue-like structures over 21 days. Upon IL-1β stimulation, the model successfully reproduced hallmarks of inflammation, including reduced anabolic markers and elevated secretion of metalloproteinases and cytokines, consistent with OA pathology. Although the current design lacks compressive loading and a 3D hydrogel matrix, its easy manipulation enables high-throughput inflammatory studies under dynamic flow, offering a more physiologically relevant environment than conventional 2D models. Key advantages include: (i) controlled mechanical stimulation *via* FSS gradients; (ii) support for cell–cell interactions and aggregate formation; and (iii) reduced consumption of cells and reagents, combined with easy operation through gravity-driven flow without pumps. This platform provides a promising tool for OA research and preclinical screening of disease-modifying osteoarthritis drugs (DMOADs). Future work should integrate 3D matrices and mechanical compression to further enhance physiological relevance and enable multi-tissue interaction studies. Furthermore, this work demonstrates the repurpose of a well-established microfluidic chip from one application to another, fostering faster progress and enhancing sustainability in OoC development.

Conflicts of interest

The authors declare no competing interests. H.-T. N., J. K., S. M., and P. S. are Finnadvance employees and shareholders.

Data availability

Data related to the manuscript has been provided both in the manuscript and the supplementary information (SI) section.

Supplementary information: Fig. S1 details the method used for fluorescence quantification. Fig. S2 presents live/dead fluorescence images acquired from the middle of a microfluidic unit containing four parallel microchannels (regions II and III) with (A) fibronectin and (B) fibronectin–collagen IV coatings. Fig. S3 shows representative fluorescence images of human articular chondrocytes cultured for 21 days in microfluidic chips, stained with TRITC-phalloidin to visualize F-actin filaments (red) and DAPI to visualize cell nuclei (blue). Videos S1–S3 display Z-stack slices obtained from fluorescence imaging. Fig. S4 shows cell viability and metabolic activity of healthy human articular chondrocytes cultured on 2D glass substrates coated with PDMS and various proteins prior to cell seeding. Fig. S5 illustrates gravity-driven flow dynamics at a 25° rocker tilt. Fig. S6 provides additional data on cell viability and metabolic activity of human articular chondrocytes cultured on 2D surfaces. Fig. S7 presents the concentration of collagen type II alpha 1 (COL2A1) secreted into the culture medium by human articular chondrocytes. See DOI: https://doi.org/10.1039/d5lc01167a.

Acknowledgements

This work received funding from The Finnish Research Impact Foundation (OASIS project, 2022-2024) as well as from Research Council of Finland (former Academy of Finland, #317437 and #320090 and #323719). Priscila Campioni Rodrigues was supported by Finnish Cultural Foundation (North Ostrobothnia Regional Fund). The authors thank Dr. Janne Koskimäki for providing access to refrigerated centrifuges at the Ecology and Genetics Research Unit, University of Oulu, and Pharmatest Services Ltd., Finland for providing access to laboratory facilities and the Q-View™ Imager LS device for Q-Plex™ assays.

References

1 Q. Liu, X. Hu, X. Zhang, X. Duan, P. Yang, F. Zhao and Y. Ao, Effects of Mechanical Stress on Chondrocyte Phenotype and Chondrocyte Extracellular Matrix Expression, *Sci. Rep.*, 2016, **6**, 37268, DOI: 10.1038/srep37268.

2 Y. Jia, H. Le, X. Wang, J. Zhang, Y. Liu, J. Ding, C. Zheng and F. Chang, Double-Edged Role of Mechanical Stimuli and Underlying Mechanisms in Cartilage Tissue Engineering, *Front. Bioeng. Biotechnol.*, 2023, **11**, 1271762, DOI: 10.3389/fbioe.2023.1271762.

3 J. Eschweiler, N. Horn, B. Rath, M. Betsch, A. Baroncini, M. Tingart and F. Migliorini, The Biomechanics of Cartilage-an Overview, *Life*, 2021, **11**(4), 302, DOI: 10.3390/life11040302.

4 N. Petitjean, P. Canadas, P. Royer, D. Noël and S. Le Floc'h, Cartilage Biomechanics: From the Basic Facts to the Challenges of Tissue Engineering, *J. Biomed. Mater. Res., Part A*, 2023, 1067–1089, DOI: 10.1002/jbm.a.37478.
5 J. D. Hunter, L. March and M. Chew, Osteoarthritis in 2020 and beyond: A Lancet Commission, *Lancet*, 2020, **396**(10264), 1711–1712, DOI: 10.1016/S0140-6736(20)32230-3.
6 F. Angelini, P. Widera, A. Mobasheri, J. Blair, A. Struglics, M. Uebelhoer, Y. Henrotin, A. C. A. Marijnissen, M. Kloppenburg, F. J. Blanco, I. K. Haugen, F. Berenbaum, C. Ladel, J. Larkin, A. C. Bay-Jensen and J. Bacardit, Osteoarthritis Endotype Discovery via Clustering of Biochemical Marker Data, *Ann. Rheum. Dis.*, 2022, **81**(5), 666–675, DOI: 10.1136/annrheumdis-2021-221763.
7 P. Carpintero-Fernández, M. Varela-Eirín, A. García-Yuste, I. López-Díaz, J. R. Caeiro and M. D. Mayán, Osteoarthritis: Mechanistic Insights, Senescence, and Novel Therapeutic Opportunities, *Bioelectricity*, 2022, **4**(1), 39–47, DOI: 10.1089/bioe.2021.0039.
8 H. Dou, S. Wang, J. Hu, J. Song, C. Zhang, J. Wang and L. Xiao, Osteoarthritis Models: From Animals to Tissue Engineering, *J. Tissue Eng.*, 2023, **14**, 1–23, DOI: 10.1177/20417314231172584.
9 S. Manivong, A. Cullier, F. Audigié, X. Banquy, F. Moldovan, M. Demoor and V. G. Roullin, New Trends for Osteoarthritis: Biomaterials, Models and Modeling, *Drug Discovery Today*, 2023, **28**(3), 103488, DOI: 10.1016/j.drudis.2023.103488.
10 N. C. Foster, N. M. Hall and A. J. E. Haj, Two-Dimensional and Three-Dimensional Cartilage Model Platforms for Drug Evaluation and High-Throughput Screening Assays, *Tissue Eng., Part B*, 2022, 421–436, DOI: 10.1089/ten.teb.2020.0354.
11 A. Weizel, T. Distler, D. Schneidereit, O. Friedrich, L. Bräuer, F. Paulsen, R. Detsch, A. R. Boccaccini, S. Budday and H. Seitz, Complex Mechanical Behavior of Human Articular Cartilage and Hydrogels for Cartilage Repair, *Acta Biomater.*, 2020, **118**, 113–128, DOI: 10.1016/j.actbio.2020.10.025.
12 A. T. Banigo, I. B. M. Konings, L. Nauta, B. Zoetebier and M. Karperien, Synthesis and Engineering of Hyaluronic Acid-Gelatin Hydrogels with Improved Cellular Attachment and Growth, *Polymers*, 2024, **16**(23), 3410, DOI: 10.3390/polym16233410.
13 Y. Fu, B. Zoetebier, S. Both, P. J. Dijkstra and M. Karperien, Engineering of Optimized Hydrogel Formulations for Cartilage Repair, *Polymers*, 2021, **13**(9), 1526, DOI: 10.3390/polym13091526.
14 A. Scalzone, G. Cerqueni, X. N. Wang, A. Ferreira-Duarte, K. Dalgarno, M. Mattioli-Belmonte and P. Gentile, An In Vitro Engineered Osteochondral Model as Tool to Study Osteoarthritis Environment, *Adv. Healthcare Mater.*, 2023, **12**(2), 2202030, DOI: 10.1002/adhm.202202030.
15 A. Atwal, T. P. Dale, M. Snow, N. R. Forsyth and P. Davoodi, Injectable Hydrogels: An Emerging Therapeutic Strategy for Cartilage Regeneration, *Adv. Colloid Interface Sci.*, 2023, **321**, 103030, DOI: 10.1016/j.cis.2023.103030.
16 D. Pereira Vasconcelos, C. Leite Pereira, M. Couto, E. Neto, B. Ribeiro, F. Albuquerque, A. Freitas, C. J. Alves, G. Klinkenberg, B. H. McDonagh, R. B. Schmid, A. M. Seitz, L. de Roy, A. Ignatius, A. M. Haaparanta, V. Muhonen, B. Sarmento and M. Lamghari, Nanoenabled Immunomodulatory Scaffolds for Cartilage Tissue Engineering, *Adv. Funct. Mater.*, 2024, **34**(29), 2400627, DOI: 10.1002/adfm.202400627.
17 M. Saranya, A. M. da Silva, H. Karjalainen, G. Klinkenberg, R. Schmid, B. McDonagh, P. P. Molesworth, M. S. Sigfúsdóttir, A. M. Wågbø, S. G. Santos, C. Couto, V. P. Karjalainen, S. D. Gupta, T. Järvinen, L. de Roy, A. M. Seitz, M. Finnilä, S. Saarakkala, A. M. Haaparanta, L. Janssen and G. S. Lorite, Magnetic-Responsive Carbon Nanotubes Composite Scaffolds for Chondrogenic Tissue Engineering, *Adv. Healthcare Mater.*, 2023, **12**(30), 2301787, DOI: 10.1002/adhm.202301787.
18 Y. Yu, J. Wang, Y. Li, Y. Chen and W. Cui, Cartilaginous Organoids: Advances, Applications, and Perspectives, *Adv. NanoBiomed Res.*, 2023, **3**(1), 2200114, DOI: 10.1002/anbr.202200114.
19 W. Lin, M. Wang, L. Xu, M. Tortorella and G. Li, Cartilage Organoids for Cartilage Development and Cartilage-Associated Disease Modeling, *Front. Cell Dev. Biol.*, 2023, **11**, 1–7, DOI: 10.3389/fcell.2023.1125405.
20 J. Männik, T. F. Teshima, B. Wolfrum, D. Yang, D. A. Ferreira, M. Rothbauer, J. P. Conde, P. Ertl, C. Oliveira, P. L. Granja, C. L. Thompson, S. Fu, M. M. Knight, S. D. Thorpe, K. Kaarj, J. Y. Yoon, H. Kamble, M. J. Barton, M. Jun, S. Park and N. T. Nguyen, Methods of Delivering Mechanical Stimuli to Organ-on-a-Chip, *Micromachines*, 2021, **8**(10), 1–14, DOI: 10.1002/advs.202003273.
21 L. Banh, K. K. Cheung, M. W. Y. Chan, E. W. K. Young and S. Viswanathan, Advances in Organ-on-a-Chip Systems for Modelling Joint Tissue and Osteoarthritic Diseases, *Osteoarthritis Cartilage*, 2022, **30**(8), 1050–1061, DOI: 10.1016/j.joca.2022.03.012.
22 C. Ma, Y. Peng, H. Li and W. Chen, Organ-on-a-Chip: A New Paradigm for Drug Development, *Trends Pharmacol. Sci.*, 2021, 119–133, DOI: 10.1016/j.tips.2020.11.009.
23 D. E. Ingber, Human Organs-on-Chips for Disease Modelling, Drug Development and Personalized Medicine, *Nat. Rev. Genet.*, 2022, 467–491, DOI: 10.1038/s41576-022-00466-9.
24 S. N. Bhatia and D. E. Ingber, Microfluidic Organs-on-Chips, *Nat. Biotechnol.*, 2014, 760–772, DOI: 10.1038/nbt.2989.
25 N. S. Bhise, J. Ribas, V. Manoharan, Y. S. Zhang, A. Polini, S. Massa, M. R. Dokmeci and A. Khademhosseini, Organ-on-a-Chip Platforms for Studying Drug Delivery Systems, *J. Controlled Release*, 2014, 82–93, DOI: 10.1016/j.jconrel.2014.05.004.
26 E. K. Sackmann, A. L. Fulton and D. J. Beebe, The Present and Future Role of Microfluidics in Biomedical Research, *Nature*, 2014, 181–189, DOI: 10.1038/nature13118.
27 N. Gupta, J. R. Liu, B. Patel, D. E. Solomon, B. Vaidya and V. Gupta, Microfluidics-based 3D Cell Culture Models: Utility in Novel Drug Discovery and Delivery Research, *Bioeng. Transl. Med.*, 2016, **1**(1), 63–81, DOI: 10.1002/btm2.10013.
28 Z. Lin, Z. Li, E. N. Li, X. Li, C. J. Del Duke, H. Shen, T. Hao, B. O'Donnell, B. A. Bunnell, S. B. Goodman, P. G. Alexander, R. S. Tuan and H. Lin, Osteochondral Tissue

Chip Derived From IPSCs: Modeling OA Pathologies and Testing Drugs, *Front. Bioeng. Biotechnol.*, 2019, **7**, 1–16, DOI: 10.3389/fbioe.2019.00411.

29 H. Tolabi, N. Davari, M. Khajehmohammadi, H. Malektaj, K. Nazemi, S. Vahedi, B. Ghalandari, R. L. Reis, F. Ghorbani and J. M. Oliveira, Progress of Microfluidic Hydrogel-Based Scaffolds and Organ-on-Chips for the Cartilage Tissue Engineering, *Adv. Mater.*, 2023, **35**(26), 1–75, DOI: 10.1002/adma.202208852.

30 D. Lee, A. Erickson, T. You, A. T. Dudley and S. Ryu, Pneumatic Microfluidic Cell Compression Device for High-Throughput Study of Chondrocyte Mechanobiology, *Lab Chip*, 2018, **18**(14), 2077–2086, DOI: 10.1039/c8lc00320c.

31 C. A. Paggi, B. Venzac, M. Karperien, J. C. H. Leijten and S. Le Gac, Monolithic Microfluidic Platform for Exerting Gradients of Compression on Cell-Laden Hydrogels, and Application to a Model of the Articular Cartilage, *Sens. Actuators, B*, 2020, **315**, 127917, DOI: 10.1016/j.snb.2020.127917.

32 C. A. Paggi, J. Hendriks, M. Karperien and S. Le Gac, Emulating the Chondrocyte Microenvironment Using Multi-Directional Mechanical Stimulation in a Cartilage-on-Chip, *Lab Chip*, 2022, **22**(9), 1815–1828, DOI: 10.1039/d1lc01069g.

33 P. Occhetta, A. Mainardi, E. Votta, Q. Vallmajo-Martin, M. Ehrbar, I. Martin, A. Barbero and M. Rasponi, Hyperphysiological Compression of Articular Cartilage Induces an Osteoarthritic Phenotype in a Cartilage-on-a-Chip Model, *Nat. Biomed. Eng.*, 2019, **3**(7), 545–557, DOI: 10.1038/s41551-019-0406-3.

34 V. Peitso, Z. Sarmadian, J. Henriques, E. Lauwers, C. A. Paggi and A. Mobasheri, Development of a Microphysiological Cartilage-on-Chip Platform for Dynamic Biomechanical Stimulation of Three-Dimensional Encapsulated Chondrocytes in Agarose Hydrogels, *Curr. Protoc.*, 2024, **4**(12), e70079, DOI: 10.1002/cpz1.70079.

35 H. Liu, X. Wu, R. Liu, W. Wang, D. Zhang and Q. Jiang, Cartilage-on-a-Chip with Magneto-Mechanical Transformation for Osteoarthritis Recruitment, *Bioact. Mater.*, 2024, **33**, 61–68, DOI: 10.1016/j.bioactmat.2023.10.030.

36 S. Grenier, M. M. Bhargava and P. A. Torzilli, An in Vitro Model for the Pathological Degradation of Articular Cartilage in Osteoarthritis, *J. Biomech.*, 2014, **47**(3), 645–652, DOI: 10.1016/j.jbiomech.2013.11.050.

37 A. Scalzone, G. Cerqueni, X. N. Wang, K. Dalgarno, M. Mattioli-Belmonte, A. M. Ferreira-Duarte and P. Gentile, A Cytokine-Induced Spheroid-Based in Vitro Model for Studying Osteoarthritis Pathogenesis, *Front. Bioeng. Biotechnol.*, 2023, **11**, 1167623, DOI: 10.3389/fbioe.2023.1167623.

38 C. I. Johnson, D. J. Argyle and D. N. Clements, In Vitro Models for the Study of Osteoarthritis, *Vet. J.*, 2016, 40–49, DOI: 10.1016/j.tvjl.2015.07.011.

39 I. Bartolotti, L. Roseti, M. Petretta, B. Grigolo and G. Desando, A Roadmap of in Vitro Models in Osteoarthritis: A Focus on Their Biological Relevance in Regenerative Medicine, *J. Clin. Med.*, 2021, **10**(9), 1920, DOI: 10.3390/jcm10091920.

40 J. Rosser, B. Bachmann, C. Jordan, I. Ribitsch, E. Haltmayer, S. Gueltekin, S. Junttila, B. Galik, A. Gyenesei, B. Haddadi, M. Harasek, M. Egerbacher, P. Ertl and F. Jenner, Microfluidic Nutrient Gradient–Based Three-Dimensional Chondrocyte Culture-on-a-Chip as an in Vitro Equine Arthritis Model, *Mater. Today Bio*, 2019, **4**, 100023, DOI: 10.1016/j.mtbio.2019.100023.

41 R. L. Smith, B. S. Donlon, M. K. Gupta, M. Mohtai, P. Das, D. R. Carter, J. Cooke, G. Gibbons, N. Hutchinson and D. J. Schurman, Effects of Fluid-induced Shear on Articular Chondrocyte Morphology and Metabolism in Vitro, *J. Orthop. Res.*, 1995, **13**(6), 824–831, DOI: 10.1002/jor.1100130604.

42 P. Wang, F. Zhu, Z. Tong and K. Konstantopoulos, Response of Chondrocytes to Shear Stress: Antagonistic Effects of the Binding Partners Toll-like Receptor 4 and Caveolin-1, *FASEB J.*, 2011, **25**(10), 3401–3415, DOI: 10.1096/fj.11-184861.

43 W. Zhong, H. Ma, S. Wang, X. Gao, W. Zhang and J. Qin, An Integrated Microfluidic Device for Characterizing Chondrocyte Metabolism in Response to Distinct Levels of Fluid Flow Stimulus, *Microfluid. Nanofluid.*, 2013, **15**(6), 763–773, DOI: 10.1007/s10404-013-1186-9.

44 B. Lazovic, H. T. Nguyen, M. Ansarizadeh, L. Wigge, F. Kohl, S. Li, M. Carracedo, J. Kettunen, L. Krimpenfort, R. Elgendy, K. Richter, L. De Silva, B. Bilican, P. Singh, P. Saxena, L. Jakobsson, X. Hong, L. Eklund and R. Hicks, Human IPSC and CRISPR Targeted Gene Knock-in Strategy for Studying the Somatic TIE2L914F Mutation in Endothelial Cells, *Angiogenesis*, 2024, **27**(3), 523–542, DOI: 10.1007/s10456-024-09925-9.

45 S. Feng, S. Mao, Q. Zhang, W. Li and J. M. Lin, Online Analysis of Drug Toxicity to Cells with Shear Stress on an Integrated Microfluidic Chip, *ACS Sens.*, 2019, **4**(2), 521–527, DOI: 10.1021/acssensors.8b01696.

46 M. Ansarizadeh, H. T. Nguyen, B. Lazovic, J. Kettunen, L. De Silva, R. Sivakumar, P. Junttila, S. L. Rissanen, R. Hicks, P. Singh and L. Eklund, Microfluidic Vessel-on-Chip Platform for Investigation of Cellular Defects in Venous Malformations and Responses to Various Shear Stress and Flow Conditions, *Lab Chip*, 2025, 10–13, DOI: 10.1039/d4lc00824c.

47 F. Khodadadei, A. P. Liu and C. A. Harris, A High-Resolution Real-Time Quantification of Astrocyte Cytokine Secretion under Shear Stress for Investigating Hydrocephalus Shunt Failure, *Commun. Biol.*, 2021, **4**(1), 387, DOI: 10.1038/s42003-021-01888-7.

48 J. Zhao, Y. Xia and J. He, Low Fluid Shear Stress Promotes Chondrocyte Proliferation and Extracellular Matrix Secretion by Downregulating Mir-143-3p and Activating the ERK5/KLF4 Signaling Pathway, *Sci. Rep.*, 2024, **14**(1), 1–13, DOI: 10.1038/s41598-024-78676-w.

49 C. B. Foldager, W. S. Toh, A. H. Gomoll, B. R. Olsen and M. Spector, Distribution of Basement Membrane Molecules, Laminin and Collagen Type IV, in Normal and Degenerated Cartilage Tissues, *Cartilage*, 2014, **5**(2), 123–132, DOI: 10.1177/1947603513518217.

50 Y. Sun, T. L. Wang, W. S. Toh and M. Pei, The Role of Laminins in Cartilaginous Tissues: From Development to Regeneration, *Eur. Cells Mater.*, 2017, **34**, 40–54, DOI: 10.22203/eCM.v034a03.

51 M. Aladal, W. You, R. Huang, J. Huang, Z. Deng, L. Duan, D. Wang, W. Li and W. Sun, Insights into the Implementation of Fibronectin 1 in the Cartilage Tissue Engineering, *Biomed. Pharmacother.*, 2022, **148**, 112782, DOI: 10.1016/j.biopha.2022.112782.

52 K. D. Roehm, I. Chiesa, D. Haithcock, R. Gottardi and B. Prabhakarpandian, A Vascularized Microfluidic Model of the Osteochondral Unit for Modeling Inflammatory Response and Therapeutic Screening, *Lab Chip*, 2024, **25**, 370–382, DOI: 10.1039/d4lc00651h.

53 H. Lin, T. P. Lozito, P. G. Alexander, R. Gottardi and R. S. Tuan, Stem Cell-Based Microphysiological Osteochondral System to Model Tissue Response to Interleukin-1B, *Mol. Pharmaceutics*, 2014, **11**(7), 2203–2212, DOI: 10.1021/mp500136b.

54 M. Rothbauer, R. A. Byrne, S. Schobesberger, I. Olmos Calvo, A. Fischer, E. I. Reihs, S. Spitz, B. Bachmann, F. Sevelda, J. Holinka, W. Holnthoner, H. Redl, S. Toegel, R. Windhager, H. P. Kiener and P. Ertl, Establishment of a Human Three-Dimensional Chip-Based Chondro-Synovial Coculture Joint Model for Reciprocal Cross Talk Studies in Arthritis Research, *Lab Chip*, 2021, **21**(21), 4128–4143, DOI: 10.1039/d1lc00130b.

55 K. W. Y. Smith, S. L. Fung, H. F. Wu, I. Chiesa, G. Vozzi, C. De Maria and R. Gottardi, Developing an in Vitro Osteochondral Micro-Physiological System for Modeling Cartilage-Bone Crosstalk in Arthritis, *Front. Immunol.*, 2025, **16**, 1495613, DOI: 10.3389/fimmu.2025.1495613.

56 F. Conceição, J. Meneses, F. Lebre, M. Becker, N. Araújo-Gomes, R. Vos, A. R. Ribeiro, E. Alfaro-Moreno, J. Leijten and L. Moreira Teixeira, Sex-Stratified Osteochondral Organ-on-Chip Model Reveals Sex-Specific Responses to Inflammatory Stimulation, *Mater. Today Bio*, 2025, **32**, 101728, DOI: 10.1016/j.mtbio.2025.101728.

57 C. Palma, S. Salehi, M. A. Polidoro, M. Moretti, M. Rasponi, S. Lopa and P. Occhetta, A Compartmentalized Joint-on-Chip (JoC) Model to Unravel the Contribution of Cartilage and Synovium to Osteoarthritis Pathogenesis, *Adv. Sci.*, 2025, **12**(42), e00374, DOI: 10.1002/advs.202500374.

58 C. Mondadori, S. Palombella, S. Salehi, G. Talo, R. Visone, M. Rasponi, A. Redaelli, V. Sansone, M. Moretti and S. Lopa, Recapitulating Monocyte Extravasation to the Synovium in an Organotypic Microfluidic Model of the Articular Joint, *Biofabrication*, 2021, **13**(4), 045001, DOI: 10.1088/1758-5090/ac0c5e.

59 L. J. Y. Ong, A. R. Sun, Z. Wang, J. Lee, I. Prasadam and Y. C. Toh, Localized Oxygen Control in a Microfluidic Osteochondral Interface Model Recapitulates Bone–Cartilage Crosstalk During Osteoarthritis, *Adv. Funct. Mater.*, 2024, **34**(28), 2315608, DOI: 10.1002/adfm.202315608.

60 A. Mainardi, A. Barbero, M. Ehrbar, M. Rasponi, I. Martin and P. Occhetta, Modular De- and Re-Construction of Vascularized Osteochondral Tissues in an Organ-on-Chip Dual-Compartment Platform, *J. Orthop. Translat.*, 2025, **56**, 101017, DOI: 10.1016/j.jot.2025.10.009.

